

Failure Analysis of Welded Steam Boiler Flange

Abdel-Aleem Hamed^{1,*}, Khodir Saad Ahmed^{1,2} and Newishy Mohamed Salah¹

¹ Welding and NDT Department, Advanced Materials Institute, Central Metallurgical Research and Development Institute (CMRDI), Helwan, P.O. Box 87, Cairo 11421, Egypt.

² The University of Bisha Faculty of Engineering, Mechanical Engineering Department, 255. Al Nakhil, Bisha 67714, Saudi Arabia

*Corresponding author: E-mail: hamedaa@gmail.com

Received 6 June 2023
Accepted 21 June 2023
Published 30 June 2023

Abstract

Steam boiler flange, made of steel ASTM A105 welded to spool pipe, experienced a failure near the welding area after six years of service. The operator company has reported that a sudden increase in operating pressure and temperature exceeded the normal operation conditions. As a result, the failed flange and welded spool pipe segments were received for further investigation using root cause analysis to determine the reason for the failure. The failed parts were visually inspected (VT) and tested for subsurface defects with a fluorescent wet magnetic particle test (MT). Chemical analysis, microstructure observations, and hardness tests are conducted for the failed flange and pipe. It is noticed that there were no abnormalities or indications of creep or overheating were found in the microstructure and hardness values. Upon examining the macro & microstructure of the connecting weld joint, several welding defects, such as non-metallic inclusions, few porosities, and lack of fusion between welded passes, were noticed. Scanning Electron Microscope (SEM) observations showed that fine striations as beach marks on the fractured surface provided strong evidence of fatigue failure. The identified crack originated from welding defects and progressed through the flange material due to fluctuating radial stresses due to the cyclic changes in working pressure during service. To prevent similar failures, it is recommended to apply proper welding procedure specifications (WPS) by qualified welders, conduct regular inspections and maintenance of the steam boiler, and keep working conditions stable.

Keywords: boiler failure, flange, welding imperfections, fatigue mechanism, un-qualified welders.

1. Introduction

Carbon steel and low alloy steels are usually used for fabricating pressure vessels and boilers due to their excellent properties, such as strength and ability to withstand corrosion and high temperatures. However, the final selection of materials for constructing pressure vessels and boilers depends on the specific requirements of the intended use and the design specifications of the equipment [1-7]. Boiler components that come into contact with steam and hot water are exposed to severe operating conditions, including high pressure, temperature, and harsh environmental conditions. These conditions play the primary role in boiler components damages such as tension-compression, corrosion fatigue, creep damage, hydrogen embrittlement, and erosion, in addition to short-term or long-term overheating and welding

defects are among the most frequent reasons for the failure of boiler components. The occurrence of stress concentration areas, such as notches, welding toes, sharp corners, keyways, dents, gouges, laps, folds, flakes, and tensile residual stresses from punched holes, heat treatment, and welding, among others, can trigger fatigue fractures [8-23].

William Liu et al. reported the failure case of creep-fatigue interaction (CFI) on a superheater in a recovery-fired boiler [19]. Two cracks were found at the weld joint's heat-affected (HAZ) zone, both of which originated from the fire-side and propagated to the steam side. The presence of beach marks on the failed fractured surface suggested that CFI caused the failure mechanism. The first crack was initiated and spread through the transgranular mode, whereas the second

crack was initiated via the intergranular mode and then progressed through a blend of intergranular and transgranular modes. This resulted in various stress levels caused by distinct modes of initiation. The primary factor leading to the fracture of CFI was the fluctuating stress, which was influenced by the hoop stress and axial stress. Hence, the fracture was attributed to the varying stress levels induced by different initiation modes. The presence of beach marks on the failed fractured surface suggested that CFI caused the failure mechanism.

After six years of service, the carbon steel flange connected to the 2-inch piping of a steam boiler experienced failure when the operating pressure and temperature surged abruptly to 2400 psi and 350°C, respectively, which exceeded the standard operating conditions of 1400 psi and 308°C. These changes in the operating pressure and temperature resulted from some troubles in the turbine, which led several times to the sudden closure of the main steam stop valve, and this led to an increase in the boiler pressure and temperature. The failure occurred adjacent to the heat-affected area of the weld joint that linked the 2-inch pipe to the flange on the side. Consequently, an investigation was conducted to determine the underlying cause of the failure. There are no data reported about the welding procedure specification (WPS), procedure qualification record (PQR), welder qualification, and welding quality control during boiler fabrication.

2. Experimental Procedure

A comprehensive analysis of the flawed piping and flange was carried out, which comprised a detailed visual inspection, non-destructive testing, and destructive testing. Chemical analysis and ultrasonic thickness measurement were conducted to assess the extent of the damage. To determine the chemical properties of the failed materials, an optical emission spectrometer was employed [21-23].

The flange material base metal, weld metal, and connecting pipe base metal were subjected to a metallographic examination near and far from the failed zone. The failed flange was sectioned utilizing a water-cooling cutting machine, and the resulting samples were prepared for metallographic analysis. The samples were examined for macro and microstructures using metallographic techniques. The process of preparing the specimens involves several steps. Firstly, they are mechanically ground down using 1200-grade emery paper. Next, they are polished with 0.1µm

agglomerated alpha alumina suspension. Then, they are rinsed and degreased with acetone. Finally, the specimens are etched for 40 seconds using a 3% Nital solution.

The hardness of the base metal (BM) of the flange and pipe, weld metal (WM), and heat-affected zone (HAZ) was assessed through a hardness test. The test was carried out following the ASTM standards E92, which pertains to the Vickers hardness test for metallic materials, and E384, which pertains to the microhardness test for metallic materials. A Scanning Electron Microscope (SEM) with Energy Dispersive X-ray Spectroscopy (EDS) analysis capability was used to investigate the fracture surface. Spot chemical analysis using EDS was performed at several points in the vicinity of the failed zone and in regions where unusual morphology in microstructure was observed. The specific SEM model used was the Quanta FEG-250.

3. Results

3.1 Visual examination

Figure 1 shows a general view of the flange and connected pipe that failed. The fracture surface was free from corrosion products and/or deposits. Figure 2 displays detailed views of the fracture initiation zone in the failed pipe. Figure 2 shows the initial fracture zone in the final filling weld layer region on the flange side, specifically at the weld toe.



Fig. 1 Fracture surface off the flange and connected pipe (as received).

The reinforcement area (final filling weld pass) seems slightly thicker than the remaining weld metal. The detailed characteristics of the damaged part of the flange are illustrated in Fig. 3, displaying the fracture initiation area, fatigue fracture (beach mark zone), and final fracture surface. As shown in Fig. 3, the original fracture surfaces at low magnification and beach marks

were noticed, indicating that the fractures were caused by fatigue and had initiated and propagated through this mechanism [27-31].

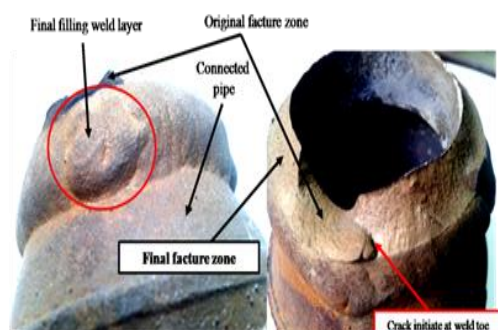


Fig. 2 Enlarged view of fractured connected pipe showing fracture initiation zone.



Fig. 3 Close-up views of the fractured section of the flange depicting the fracture initiation zone, the fatigue fracture or beach zone, and the final fracture surface.

The fatigue region of the fracture surface appeared smooth, while the remaining area corresponding to the final and rapid fracture exhibited the typical features of a brittle fracture, with minimal or no evidence of plastic deformation. No cracks were observed near the ruptured areas, and there was no damage or loss of thickness (8mm) in the flange wall.

3.2. Results of magnetic particle testing (MT)

Figure 4 shows the inner surface of the cross-section of the axially welded joint between the flange and the connected pipe. It revealed a non-acceptable High side while the other side is low (HI-LO) by almost (4mm) on the inner surface of the weld joint. Such types of imperfection may disrupt the movement of fluids such as water or steam, resulting in mechanical stress on the welded area. However, examining the flange and linked

pipe's internal surface using magnetic particle testing (MT) did not reveal any signs of corrosion or pitting, indicating the efficacy of the water treatment process.

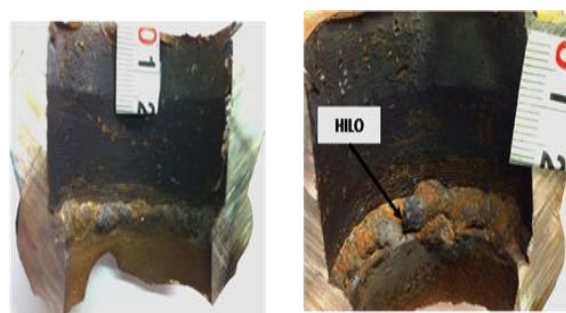


Fig. 4 Mismatch fitting of Hi-Lo at the internal surface of the weld connecting steel to flange

3.3. Chemical analysis

The chemical composition of the flange, weld metal, and connected pipe is shown in Table 1 and confirmed with the specifications given in Table 2 for ASTM A105.

Table 1 Chemical composition of the received flange.

Steel type	Chemical composition (mass%)											
	C	Si	Mn	P	S	Cr	Mo	Ni	Cu	V	B	Fe
Received flange	0.172	0.308	0.87	0.005	0.003	0.1	0.02	0.09	0.27	0.004	0.0003	98.09
Weld metal	0.09	0.84	1.37	0.001	0.018	0.018	0.006	0.038	0.13	0.007	0.003	97.44
Connected pipe	0.22	0.21	1.13	0.022	0.031	0.021	-	0.014	0.031	0.005	0.0005	98.22

Table 2 chemical composition of ASTM A105.

Steel type	Chemical composition of ASTM A-105 (mass%)											
	C max	Si	Mn	P max	S max	Cr max	Mo max	Ni max	Cu max	V max	B max	Fe
A-105	0.35	0.1-0.35	0.6-1.05	0.035	0.04	0.3	0.12	0.4	0.4	0.05	0.02	Bal.

3.4 Macrostructure investigations

Figure 5 shows the macrostructures of the weld joint's as-polished and etched cross-section near where the fatigue fracture originated (i.e., the final filling weld layer). As shown, revealed several welding defects, including porosity, slag inclusion, and lack of fusion at the boundary line between the initial and final weld passes. These findings provide evidence of the substandard quality of the weld joint. The corresponding microstructures of the specimens can be shown in Figs 6 and 7.

3.5 Microstructure investigations

The microstructure of the flange material (ASTM A105 alloy) base metal (BM) reveals ferrite-lamellar pearlite, which can be seen in Figure 7a. No signs of

overheating were observed, such as creep indications or noticeable plastic deformation leading up to the fracture. The heat-affected zones (HAZ) have microstructures that include pearlite-upper bainite and tempered ferrite-pearlite, depicted in Figs. 7b and 7c, correspondingly.

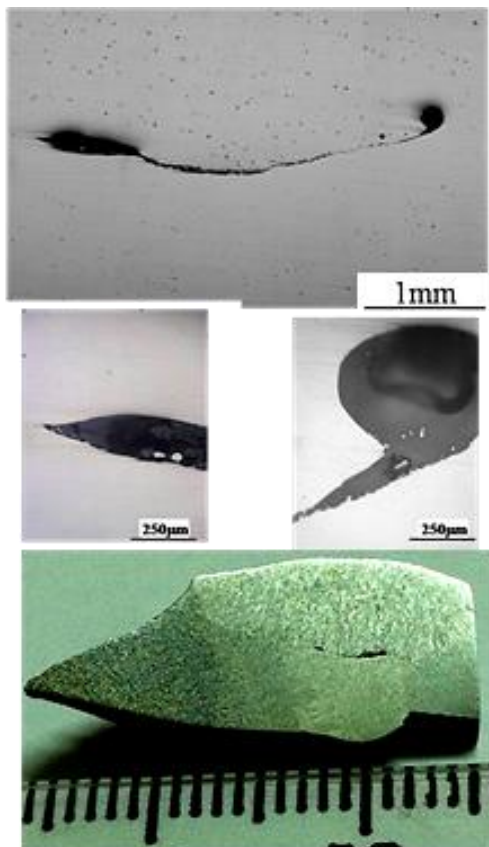


Fig. 5 Macrostructure of the welding cross-section reveals internal flows at the boundary line between inter-passes. (as-polish and etched)

The microstructure of the base metal of the connected pipe shows an acicular ferrite-pearlite structure, as shown in Figure 7d. Figure 7e shows the microstructure of the final layer's weld metal (WM), which contains acicular ferrite, side plate ferrite, and grain boundary ferrite. The initial layer, known as the root pass, has annealed ferrite-pearlite structures, as seen in Figure 7f. The grain size of the heat-affected zone (HAZ) is coarser near the fusion line and gradually becomes finer as it moves further away from it.

The microstructure of the base metal of the connected pipe shows an acicular ferrite-pearlite structure, as shown in Figure 7d. Figure 7e shows the microstructure of the final layer's weld metal (WM), which contains acicular ferrite, side plate ferrite, and

grain boundary ferrite. The initial layer, known as the root pass, has annealed ferrite-pearlite structures, as seen in Figure 7f. The grain size of the heat-affected zone (HAZ) is coarser near the fusion line and gradually becomes finer as it moves further away from it.

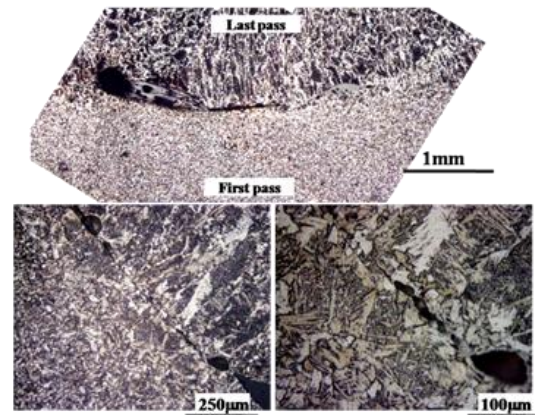


Fig. 6 Microstructures of the cross-section of the weld metal showing several internal defects.

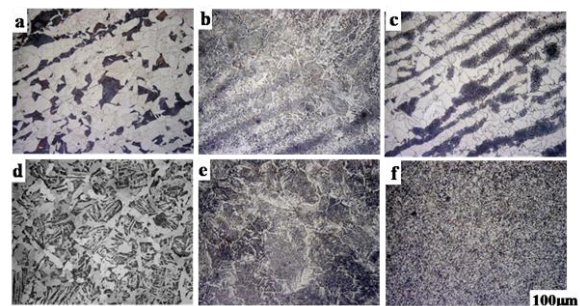


Fig. 7 Microstructures of different areas of weld joint showing: (a). flange (BM), (b), (c) HAZ of the weld joint, (d) BM of welded pipe, (e) final pass (cap pass), and (f) root pass of the weld.

3.6 Scanning electron Microscopy (SEM) investigation

The fracture surface was investigated using a Scanning Electron Microscope (SEM) showed the presence of striation marks, which indicated that the fractures had resulted from fatigue and had progressed over time, as depicted in Fig. 8. An Energy Dispersive Spectroscopy (EDS) analysis equipped with the SEM is used to examine the original fatigue fracture surface, as shown in Fig. 9. The analysis results indicated that harmful elements, such as Cl, S, Ca, K & Na, were absent.

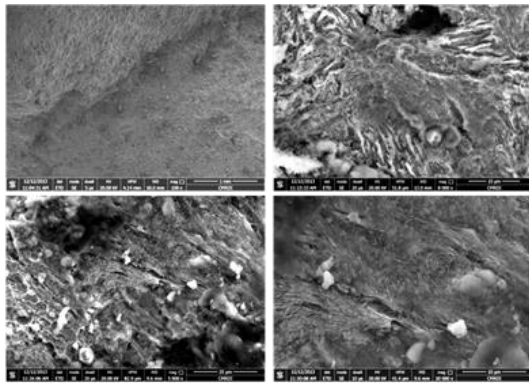


Fig. 8 Scanning electron microscope (SEM) images of the original crack initiation zone showing fatigue striations.

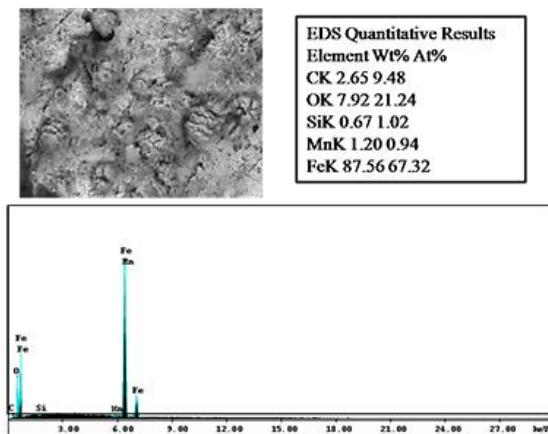


Fig. 9 Results EDS analysis of SEM and at the original fracture surface.

3.7 Hardness measurements

Table 3 shows the Vickers hardness measurements, which were taken along the cross-section transverse to the welding direction under a load of 9.8N for a loading time of 15 seconds. The hardness values for the flange (BM), flange (HAZ), (WM) of the cap pass of the last weld layer, (WM) first layers, connected pipes (BM), and connected pipe HAZ were 180, 210, 220, 195, 205, and 220Hv, respectively. These measurements confirm that the weld joint was free from any creep effects, indicating its soundness.

Table 3 Hardness of different steel pipes.

material & location	Flange material		Weld metal		Connected pipe	
	BM	HAZ	first layer	last layer	BM	HAZ
Hardness Hv	180	220	194	220	202	215

4. Discussions

The material was found to conform to the ASTM A105 specification, with typical microstructure and hardness values and no abnormalities or indications of creep, thus ruling out the possibility of overheating. Additionally, no cracks were observed near the fracture area, eliminating the possibility of the flange material being defective or overstressed. The fracture surface of the flange appears to have occurred due to fatigue cracks initiated near or at the toe of the weld, a high-stress concentration area, caused by welding defects. Examination of the macro and microstructures of the weld joint (Figs. 5, 6) revealed several welding defects at the fusion of the boundary between the root pass and final filling passes of the weld layer, as shown in Fig. 2. The crack began at the weld's toe and proceeded through the flange material, caused by the fluctuating radial stresses resulting from the fluctuating working pressure during service, with increasing and decreasing values.

The EDS analysis conducted on the fracture surface showed the existence of carbon, silicon, manganese, oxygen, and iron. Examination under a Scanning Electron Microscope (SEM) revealed the presence of fine striations in the beach mark areas of the broken flange, indicating a fatigue failure. The ultimate tensile strength of the flange material was suddenly surpassed when the operating pressure rose sharply, causing the final fracture, which had lower hardness values than the connected pipe material (as seen in Table 3).

Fatigue fractures are known to occur when a steel flange undergoes cyclic variations in stress, which lead to the development of fractures below its yield strength. The critical factors that lead to fatigue fractures include high tensile stress, significant stress variations, and numerous stress cycles [9, 10]. As shown in Figs. 4 and 5, weld quality such as Hi-LO, irregular bead, and un-uniform heat inputs distributions inside the weld groove during welding sequences passes lead to stress concentration areas that can trigger fatigue fractures. Visible beach marks can indicate the location of fracture initiation. These marks form when oxidation at the crack tip propagates under alternating stress and is occasionally interrupted, such as when working pressure varies during service. Visible beach marks also occur during non-steady-state loading or rapid changes in loading, such as when a boiler is turned on and shut down.

In flange materials such as steel A105 with ductile properties, crack propagation occurs through the coalescence of microvoids, resulting in a crack path direction perpendicular to the applied tensile axis. The correlation between the striations spacing and applied tensile load has been well investigated, where each

striation represents one fatigue load cycle. As the maximum tensile loading increases, the spacing between striations also increases. In the weld metal section near the weld toes of the final filling weld area, there was evidence of weld defects such as lack of fusion, slag inclusion, and porosity. The fatigue cracks continued to propagate until the thickness of the cross-section of the steel flange was insufficient to support the increasing working pressure (2400psi), which exceeded the design limit of 1400psi. The fracture surface reveals that cracking occurred under radial tensile stresses.

5. Conclusion

According to the main results of this investigation, the failure of the steel flange resulted from fatigue failure caused by improper welding practices during the connection of the flange to the connected pipe. The presence of porosity, lack of fusion, and non-metallic inclusions near the welding toe may have contributed to the initiation and propagation of cracks, ultimately leading to fatigue failure in the cap pass area. Implementing appropriate welding procedures with corresponding Welding Procedure Specifications (WPS) and Procedure Qualification Records (PQR) is strongly recommended, and qualified welders should carry out the welding according to ASME code section IX (boiler pressure vessel code). In addition, non-destructive testing (NDT) should be conducted post-welding to ensure the integrity of the weld. Welding technique should be performed without developing stress concentration areas such as high reinforcement, irregular bead, and Hi-Lo to decrease fatigue failure in case of abruptly increasing / or decreasing of working pressure and temperature.

References

- [1] A. D. Nugraha, Evaluation of Cyclic Tensile Stress Effect in Boiler Tube Failure. In Defect and Diffusion Forum. Trans Tech Publications Ltd, 415, (2022)115-120.
- [2] A. D. Nugraha and M. A. Muflikhun, Failure in power plant system related to mitigations and economic analysis; A study case from steam power plant in Suralaya, Indonesia. Results in Engineering, 17, (2023) 101004.
- [3] B. Guo, Baichen, Y. Zhu, L., Dai, C., Deng, H., Peng, D. Wang, and H. Liang, Stress state at the root of variable-wall-thickness pipeline welded joint. International Journal of Pressure Vessels and Piping, 200, (2022) 104785.
- [4] S. Suwarno, A. Jabar I'jazurrohman, F. Dwi Yudanto and V.S. Djanali, Failure analysis of waste heat boiler tubing caused by a high local heat flux, Eng. Failure Anal. 136, (2022) 106147
- [5] W., Abd-Elaziem, M., Khder, M. Newishy and H. Abdel-Aleem, Metallurgical characterization of failed A106 Gr-B carbon steel welded condensate pipeline in a petroleum refinery. Journal of pressure vessels and piping, 200, (2022) 104843.
- [6] M. Sattar, A. Othman, S. Kamaruddin, M. Akhtar, R. Khan, Limitations on the computational analysis of creep failure models: a review, Eng. Fail. Anal. 134, (2022) 105968.
- [7] M. B. Lin, K. Gao, C. J. Wang, and A. A. Volinsky, Failure analysis of the oil transport spiral welded pipe. Eng Fail Anal, 25, (2012)169-74.
- [8] M. Khider, W. Abde_Elaziem, M. Newishy and H. Abdel-Aleem, Metallurgical analysis of ASME SA 213 T12 boiler vertical water-wall tube failure. Eng Fail Anal., 145, (2023) 107016.
- [9] C.A. Duarte, E. Espejo, J.C. Martinez, Failure analysis of the wall tubes of a water-tube boiler. Eng. Fail. Anal., 79, (2017) 704–713.
- [10] S.A. Khodir and H. Abdel-Aleem, Localized corrosion failure of type 316 stainless steel drain pipe line. Materials performance, 55(9), (2016) 54-57.
- [11] S. Xue, R. Guo, F. Hu, K. Ding, L. Liu, L. Zheng and T. Yang, Analysis of the causes of leakages and preventive strategies of boiler water-wall tubes in a thermal power plant. Eng. Fail. Anal, 110, (2020) 104381.
- [12] J. Li., P. Zhou, G. Yu, H. Yan, Z. Chen, G. Song, and Z. Liao, Failure analysis of the water-wall tube in KIVCET waste heat boiler. Eng. Fail. Anal., 121, (2021) 105–155.
- [13] W. Liu, Failure analysis on the economisers of a biomass fuel boiler, Eng. Fail. Anal., 31, (2013) 101–117.
- [14] D.R.H. Jones, Creep failures of overheated boiler, superheater and reformer tubes. Eng. Fail. Anal. 11 (6), (2004) 873–893.
- [15] C. Barbosa, S.K. de Barros, I. de Cerqueira Abud, J.L. Do Nascimento, and S.S. de Carvalho. Failure analysis of an aqua tubular boiler tube, J. Fail. Anal., 12 (6), (2012) 654–659.
- [16] J. Ahmad, J. Purbolaksono, and L.C. Beng, Thermal fatigue and corrosion fatigue in heat recovery area wall side tubes. Eng. Fail. Anal. 17 (1), (2010) 334–343.
- [17] S. Xu, C. Wang, W. Wang, Failure analysis of stress corrosion cracking in heat exchanger tubes during start-up operation. Eng. Fail. Anal. 51, (2015) 1–8.
- [18] M.M. Rahman, J. Purbolaksono, and J. Ahmad, Root cause failure analysis of a division wall superheater tube of a coal-fired power station. Eng. Fail. Anal. 17 (6), (2010) 1490–1494.

- [19] W. Liu, A superheater creep-fatigue interaction failure and its stress assessment, *Eng. Fail. Anal.* 119, (2021) 105004.
- [20] P. Munda, S. Kumar, A. Prakash, M. Husain, V. Rajnikanth, and S.C. Ghosh, Failure investigation of boiler water wall tubes of a thermal power station, *J Fail. Anal. Preven.* 16, (2016) 9–18.
- [21] A. Firouzeh, K. Ranjbar, S. Lari Baghal, A. Heidari Kaidan, and E. Mohemi, Failure assessment of ASTM A213–T12 superheater boiler tubes in a natural gas liquid plant, *Eng. Fail. Anal.* 89, (2018) 15–27.
- [22] M. Song, T. Xu, K. Yuan, H. Yu, and C. Sun, Creep failure of a steam pipe girth weld and NDT strategy on creep damage, *Eng. Fail. Anal.* 104, (2019) 673–681.
- [23] ASTM E3 – 01 Standard Guide for Preparation of Metallographic Specimens, ASTM International, (2004).
- [24] *Metals Handbook; Welding and Soldering*, ASM. Vol. 6 (2002).
- [25] *Metals Handbook; Welding and their Weldability*. AWS Vol. 4 (1982).
- [26] *Metals Handbook; Failure Analysis and Prevention*, ASM. Vol. 11(2002).
- [27] T. B. William. ASM International Course 0335, Principles of Failure Analysis, Lesson 3: Ductile and Brittle Fracture, Page 61- 63.
- [28] Davis, J.R., Principles, and Procedures of Fractography in *Metals Handbook, Desk Edition*, 2nd Edition, ASM International, (1998) 1238-1247.
- [29] P. N. Rao, *Manufacturing Technology – foundry, forming and welding*, McGraw Hill Publisher, (2018).
- [30] Y. Bai and B. Qiang, *Subsea Pipelines and Risers*, Elsevier Inc, USA, (2005).
- [31] A. Dhooge and E. Deleu, Susceptibility of Brittle Fracture of Flanges in ASTM A105 In Proceedings of the Seminar, Progress in European Research on Major Accidents Hazards'. Fed. Ministry of Employment and Labour, Antwerpen Research Center of Belgian Welding Institute (BWI). 10.10. (2001).